LBL-11013
Preprint

Lawrence Berkeley Laboratory
UNIVERSITY OF CALIFORNIA

ENERGY & ENVIRONMENT DIVISION

Submitted to Combustion and Flame

FLAME PROPAGATION IN GRID-INDUCED TURBULENCE

R.G. Bill, Jr., I. Namer, L. Talbot, R.K. Cheng,
and F. Robben

June 1980

Prepared for the U.S. Department of Energy under Contract W-7405-ENG-48

DISCLAIMER

FLAME PROPAGATION IN GRID-INDUCED TURBULENCE

R. G. Bill, Jr.[†], I. Namer[††], L. Talbot

Department of Mechanical Engineering
University of California
Berkeley, California 94720

R. K. Cheng and F. Robben

Lawrence Berkeley Laboratory
Berkeley, California 94720

The interaction of grid-generated turbulence with premixed, V-shaped ethylene/air flames has been studied using laser Doppler anemometry and Rayleigh scattering as optical diagnostics respectively for the streamwise component of velocity and the density. Turbulent flame propagation was studied for three upstream flow velocities, U_∞ = 245, 500, and 684 cm/s with fuel/air equivalence ratios ranging from 0.55 to 0.75. The angle of the flame with the flow axis was varied from 12° to 24°. Profiles of mean values and the turbulence intensity of velocity and density were obtained through the flame. For all conditions, the turbulence intensity of velocity was observed to decrease behind the flame indicating the dominance of dilatation effects. In addition profiles of the mean streamwise velocity component indicate streamlines to be significantly deflected at the flame for the case of the most oblique flame. For the conditions in which the flame angle was 12°, the wake of the flame-holder dominates the flow field behind the flame and vortices are observed. This suggests that results for these conditions are not typical of the interaction of a flame with grid-induced turbulence. Probability density functions of Rayleigh scattering in the flame and turbulent intensities indicate that intermediate states of chemical species are likely to be significant in determining density statistics.

[†]Present address: Department of Mechanical Engineering, Columbia University, New York, N.Y.

[††]Present address: Department of Mechanical Engineering, Drexel University, Philadelphia, PA

1. INTRODUCTION

Although considerable attention has been given to the study of turbulent flame propagation since the pioneering work of Damkohler [1], lack of velocity, density (temperature) and species concentration data have critically impeded progress in our understanding of the interaction of combustion and turbulence. Questions concerning the effect of combustion on mean streamlines, turbulent kinetic energy and turbulent length scales remain unanswered. The effects of different turbulent eddy scales and their associated kinetic energy on flame propagation speed are also unknown. Models of turbulent flame propagation [2,3,4] have focussed attention on these problems; however, little data is available to guide theorists in their choice of proper models in turbulent combustion. Our study of flame propagation in low intensity grid-generated turbulence using laser-Doppler anemometry (LDA), and Rayleigh scattering provides data on the effect of combustion on turbulent kinetic energy and flow divergence.

Early models of turbulent flame propagation based upon mixing length and other ad-hoc arguments had limited success in correlating available data. The inability of the wrinkled laminar flame models of Damkohler [1] and Shchelkin [5] to correlate turbulent flame speeds resulted in the proposal by Karlovitz et al. [6] that additional turbulence was generated by the combustion process itself. However, Richmond et al. [7] and Smith and Gouldin [8] have shown that large errors in measurement in flame speed may result if local velocity measurements are not made at the flame front. This observation, as well as our results which do not show an increase in turbulent kinetic

energy, suggest that the lack of correlation may in part be due to errors in measurement of the flame speed.

More recent models of turbulent flame propagation [2,3,4] have sought to more systematically calculate the effect of turbulence on combustion using the conservation equations. Clavin and Williams [4] developed a statistical theory for the structure and propagation velocity in turbulent flows with length scales large compared with the laminar flame thickness. The analysis involves a regular perturbation for small value of the ratios of the laminar flame thickness to the turbulent length scale. This approach is superior to that of previous phenomenological models in that it is not necessary to introduce arbitrary assumptions concerning the flame shape. The turbulent burning rate appears as a solution to an eigenvalue problem for a given fluctuating flow field. The model is limited in that the density change associated with heat release is neglected. However, the qualitative features resulting from the method of formulation are still of interest. The model predicts a functional form for the burning speed consistent with the wrinkled-laminar flame model. No dependence on length scale is indicated. (We note this contradicts the correlation of Andrews et al. [9]). Since the velocity flow field is assumed to be given, no information on the effect of combustion on turbulent kinetic energy can be obtained.

Bray and Libby [2] in a study of turbulence-combustion interactions in premixed flows calculated the effect of heat release on turbulent flame speed and kinetic energy. The statistical model employs density weighted averaging to take into account variations in density due to

heat release. A probability density function dependent on a single reaction progress parameter and location is used to compute statistical moments related to concentration fluctuations. The model predicts that turbulent kinetic energy will be reduced by dilatation effects for flames nearly normal to the upstream flow direction. At higher angles, turbulent kinetic energy is predicted to increase due to shear. This model assumes that the streamlines remain undeflected through the flame. The imposition of this condition causes the model to predict a significant Reynolds stress in the flame and an increase in turbulent kinetic energy due to the interaction of this stress with the velocity gradient. The flame speed, as in Clavin and Williams [4], is found to be independent of the upstream length scale. In a subsequent paper, Libby and Bray [3] predict that the effects of variations in density are important in the modelling of turbulent transport terms such as the Reynolds stress.

In our studies of turbulent flame propagation, we have used Rayleigh scattering and LDA in the turbulent combustion regime corresponding to the wrinkled laminar flame. A V-shaped C_2H_4/air flame was stabilized on a rod downstream of a grid used to generate turbulence. For flames at relatively large angles to the flow, the effect of heat release and flow dilatation is to decrease turbulent kinetic energy. At smaller flame angles, however, no increase in turbulent kinetic energy was detected. This is in contradiction to the results of Bray and Libby [2], and would seem to indicate that their assumption of undeflected streamlines is a poor approximation for unconfined flames in low turbulence flows. In addition, as suggested by Smith

and Gouldin [8], the measured increases in turbulent kinetic energy due to the wake of the flame holder indicate that at high velocities the results are more representative of the interaction of a flame with wake-generated turbulence.

2. EXPERIMENTAL TECHNIQUES

Experimental Apparatus

In Figure 1 a schematic is shown of the experimental apparatus. A coaxial jet is used in which the premixed gases of ethylene and air flow through the central jet, surrounded by an outer coaxial jet, used to shield the inner flow from mixing with the stagnant surroundings. The inner and outer jet diameter were 5.1 cm and 10.2 cm respectively. The flow velocity of the inner and outer jets were matched using the output of a calibrated DISA hot-wire 55P11 and 55D01 anemometer system. The flow rates were also monitored using standard rotameters.

A bi-plane, circular grid was placed 5 cm upstream of the exit of the coaxial jet to generate turbulence. For all conditions described below, the mesh size of the grid, M, was 0.5 cm and the grid elements were 0.1 cm in diameter. A V-shaped flame was stabilized on a 0.1 cm diameter rod positioned at the exit of the nozzle as shown in Figure 1. In the coordinate system used throughout, the x-coordinate is parallel to the jet axis and the y-coordinate is normal to the jet axis with the origin at the center of the grid. During a typical measurement

sequence, the experimental apparatus was fixed at a given x-location and traversed by computer control in the y-direction to provide profiles of velocity and of Rayleigh scattering.

Rayleigh Scattering

Rayleigh scattering in gases results from the inhomogeneous nature of the medium produced by fluctuations in the dielectric constant. The Rayleigh scattering intensity is related to the gas density by

$$I_R = C\, I_o\, N \sum_i X_i\, \sigma_{Ri} \qquad (1)$$

where I_R is the intensity of Rayleigh scattered light, C a calibration constant of the optics, I_o the incident laser light intensity, N the total molecular number density, X_i the mole fraction of chemical species i and σ_{Ri} the Rayleigh cross-section for the i^{th} species. The above expression (1) indicates that I_R will depend on the degree of reaction through species-dependent terms. A study of this effect for typical combustion cases (Namer et al. [10]) has shown that Rayleigh scattering for ethylene/air mixtures may be interpreted as proportional to gas density, ρ, to an accuracy of better than 5% for the conditions of this study. Therefore non-dimensionalizing (1) by a reference condition denoted by subscript ∞ :

$$\frac{I_R}{I_\infty} = \frac{N}{N_\infty} \frac{\sum_i x_i\, \sigma_{Ri}}{\left(\sum_i x_i\, \sigma_{Ri}\right)_\infty} \simeq \rho/\rho_\infty \qquad (2)$$

The optical system for Rayleigh scattering is similar to that employed by Cheng et al. [11,12]. A Spectra Physics 4-watt Argon ion laser is used as the light source for both the Rayleigh scattering and LDA measurements. The laser beam is focussed to 40 micron waist diameter by two lenses and the scattering is collected at 90° from the beam direction by an f/1.2, 55 mm focal length camera lens used at f/2.7 effective aperture in order to provide sufficient clearance. The collected light passes through a 50 micron slit, is collimated, and then filtered by a 1.0 nm band-pass filter centered at 488 nm. The collected light is then refocussed to the surface of a RCA 931A type photomultiplier. The photomultiplier output is amplified by an electrometer with a band-pass from dc to 1.9 KHz (3 db corner frequency).

Laser Doppler Anemometry

The LDA system used is of intersecting dual-beam type with real fringes (Durst et al. [13]). An equal path length beam splitter with fixed separation of 5 cm is used, and the two laser beams are focussed by a 250 mm focal length lens to form the scattering volume. Seed particles are generated by a cyclone-seeder using Al_2O_3 particles nominally 0.3 micron in diameter. Scattering bursts from the particles are collected at 90° from the forward scattering direction by a lens, filter and photomultiplier assembly and the Doppler frequency is obtained using a TSI 1090 frequency tracker. In order to consider the output of the frequency tracker as a continuous signal, it was necessary to have sufficient particles in the flow to provide the tracker with a high data rate as compared with the highest frequency fluctuation in the

flow. With an exit nozzle velocity of 245 cm/s, the data rate was typically greater than $5x10^3$ s^{-1}. At the higher velocities, the number was greater than $2x10^4$ s^{-1}. At such high data rates, it can be assumed that tracker output is essentially continuous and may be treated in a manner analogous to that of a hot wire signal. Inspection of calculated power spectra confirms this point.

Computerized Data Acquisition

To facilitate the use of the above optical systems a computerized data acquisition system based upon a Digital Equipment Corporation (DEC) PDP 11/10 was employed. The computer system is operated under DEC RT-11 using an RK05 disk with 1.25 million (16 bit) words and two IBM 729 magnetic tape drives. The experimental apparatus, mounted on a three-axis traverse, was positioned by computer controlled stepping motors, so that flow field positions for Rayleigh scattering and LDA measurements were scanned automatically. Measurements were obtained using a 12 bit A/D converter. Samples were acquired at a constant sampling rate of 4000 or 2000 s^{-1}. Raw data were stored on a 7-track magnetic tape for post-processing with either the PDP 11/10 or the Lawrence Berkeley Laboratory CDC 7600.

The mean values and turbulence intensity were calculated from the time series of the Rayleigh scattering and LDA data. The time series consisted of 5000 samples of the analog signals taken at 4000 s^{-1} for upstream flow velocity U = 684 cm/sec. At the lower velocites samples were acquired at a rate of 2000 s^{-1} rate. The LDA signal obtained from the TSI 1090 frequency tracker was filtered with an RC low pass

filter, with corner frequencies of 2 KHz or 1 KHz depending on whether the sampling rate was 4000 or 2000 s^{-1}.

Data Reduction Techniques

To determine the turbulence fluctuation intensities of Rayleigh scattering and velocity measurements, the electronic noise associated with the photomultiplier and frequency tracker must be removed. In the case of Rayleigh scattering, the variance of the noise of the photomultiplier is proportional to the mean current (Robben [14]). Therefore at the beginning of each profile, photomultiplier fluctuations in the free stream outside the flame were recorded. Since no density fluctuations exist at this location, the signal variance is due primarily to photomultiplier noise. Then at other locations this variance, adjusted for change in the mean current level of the photomultiplier, is subtracted from the total signal variance. In addition to this error, the mean signal level related to Rayleigh scattering may be contaminated with unrelated background light picked up by the collection optics. This background intensity was measured by moving the collection optics $\pm$ 0.38 mm in order to allow the slit to block light scattered directly from the laser beam. The electrometer output measured in this manner was subtracted from the total mean signal. The resultant output is then proportional to the Rayleigh scattering.

The noise associated with the LDA frequency tracker arises from several sources: tracker broadening, and general instrumentation noise. The noise variance was determined by measuring the velocity variance in a laminar jet, i.e. a flow in which the turbulence intensity

was approximately 0.5%. The noise level measured in this manner corresponded to a velocity variance of 14.6 $(cm/s)^2$. This level, which was subtracted from the total variance, is typically less than 10% of the total variance measured under turbulence conditions in which U = 684 cm/s or 501 cm/s. At the lower velocity, U = 245 cm/s, this level is approximately 15% of the variance. Comparison of results for grid-turbulence without combustion (see below) and previously reported results indicate that this technique of noise removal is adequate.

3. RESULTS

Grid-Generated Turbulence

One of the classical problems in fluid mechanics is that of grid-generated turbulence. The problem is attractive since many of the general features of turbulence are exhibited, while the flow description is simplified in that the turbulence may be approximated as isotropic. Batchelor and Townsend [15] showed experimentally that $\overline{U}^2/\overline{u'^2}$ is proportionally to x/M, where $\overline{U}$ and u' are respectively the mean and fluctuating component of the streamwise velocity; x is the downstream coordinate and M is the grid mesh size. This result is independent of U for similar grids apart from small random changes in the virtual origin of turbulence occurring for different mesh Reynolds number $Re_M = UM/\nu$.

The Taylor microscale, λ, an approximate length scale for

dissipation is defined by the equation:

$$\overline{\left(\frac{\partial u'}{\partial x}\right)^2} = \frac{\overline{u'^2}}{\lambda^2} \tag{3}$$

A consequence of the turbulent kinetic energy balance and the linearity of $\overline{U}^2/\overline{u'^2}$ with x/M is the result:

$$Re_\lambda = \frac{\sqrt{\overline{u'^2}}\,\lambda}{\nu} = \text{const (independent of x for a given } R_M).$$

These results have been tested by Batchelor and Townsend over the range, $600 < Re_M < 4.4 \times 10^4$ and $25 < x/M < 150$. In Figure 2, $\overline{U}^2/\overline{u'^2}$ is plotted versus x/M for the three inlet velocities of this study. At a given location x/M, $\overline{U}^2/\overline{u'^2}$ is calculated from the data of 20 points spaced at 1 mm intervals across the center of the grid. As predicted for isotropic turbulence, the slopes are approximately constant. As with the data of Batchelor and Townsend [15], no systematic shift in the origin of turbulence is apparent with changing flow velocity. Hence the result, as in previous studies, appears to be quite sensitive to slight changes in inlet conditions.

The average slope of the lines in Figure 2 is 92. The data of Batchelor and Townsend [15] give an average slope of 134. The ratio of the mesh size to mesh element diameter, M/d, for their experiment is 5.3 as contrasted with 5.0 for the present study. As noted by Bathelor and Townsend [15] considerable scatter exists in the literature. Von Kármán [16] for M/d = 4.76 found the slope to be 99. Thus considering the

close proximity of our measurements to the grid, our results seem quite reasonable.

Taylor's hypotheses may be used to calculate λ from equation (3) (see e.g. Bennet and Corrsin [17]), i.e.

$$\frac{\overline{u'^2}}{\lambda^2} = \frac{1}{\overline{U}^2}\left(\overline{\frac{\partial u'}{\partial t}}\right)^2 \quad . \tag{4}$$

Over the relatively narrow range in Re_M and x/M which was investigated, λ is found to be approximately 0.2 cm. Andrews et al. [9] have correlated turbulent flame speeds with Re_λ. For $Re_\lambda < 100$, they suggested a wrinkled laminar flame model was appropriate. Our data covers the range $10 < Re_\lambda < 30$.

Experimental Conditions for Flame Propagation Studies

Turbulent flame propagation was studied for three flow velocities U = 245, 500, and 684 cm/s. The equivalence ratios were adjusted for the three velocities to provide a flame half angle, α, of approximately 24° as measured from the flow centerline. The equivalence ratios for these three cases were respectively 0.55, 0.7 and 0.75. At the highest flow velocity (684 cm/s), additional measurements were obtained at equivalence ratios of 0.6 and 0.7, which gave flame half angles of approximately 12° and 18° respectively. The mean flame front position was defined as the point at which the root mean square (rms) of the

fluctuations in density reached a maximum. This definition was found to be approximately equivalent to that of Smith and Gouldin [8] in which the mean flame front position was defined as the mean isotherm twice the value of the ambient absolute temperature. In Figure 3, a photograph of the flames corresponding to the conditions U = 684 cm/s, ϕ = 0.6, 0.7, 0.75 is shown. We note that the flame angles measured from Figure 3 are within 1° of those measured by Rayleigh scattering. Table 1 summarizes these conditions along with the associated mesh Reynolds number $Re_M = \frac{UM}{\nu}$.

Results and Observations of Flame Propagation Studies

Rayleigh scattering measurements for the conditions of Table 1 provide data for mean density profiles, flame location, and density fluctuation intensities. A typical profile of the Rayleigh scattering level and fluctuation intensity level is shown in Figure 4, with the y-coordinate normalized by the flame holder diameter (d = 1 mm). These results correspond to the flow condition, U = 684 cm/s, ϕ = 0.75, and x = 7.5 cm. The relative level of Rayleigh scattering has been interpreted as the ratio of the local gas density to the gas density in the free stream.

The rms fluctuations shown in Figure 4 are primarily due to the random movement of the flame sheet across the probe volume. The maximum turbulence intensity of 33% is typical for all results. The effect of turbulence fluctuations in the density profile is seen most markedly in the increase in mean flame thickness. While the laminar

flame thickness is less than 1 mm for these conditions, the flame thickness here is approximately 4 mm. The flame thickness was seen to increase with distance x, varying from 3-5 mm. The increase in thickness would appear to result from the extension beyond the flame holder of the flame into the field of grid-generated turbulence, see Figure 3.

The probability density function (p.d.f.) plotted in Figure 5 was calculated from the electrometer-amplified photomultiplier output for the conditions of maximum turbulent intensity in Figure 4. The distribution is highly bimodal. The highest probability densities are for cold reactants and for completely burned products. Since the chemical reaction rates are quite high, the probability of an intermediate state is low. In the p.d.f. this intermediate state may be overestimated since the response time of the Rayleigh signal is limited by the bandpass of the electrometer. The probability of intermediate states is indicated to be about 40%. Libby and Bray [3] have predicted the intensity of turbulence as a function of heat release using a p.d.f. that neglects intermediate states. For the conditions of Figure 4, they predict $\overline{\rho'^2}/\rho_\infty = .43$ in contrast to our value of .33. Nevertheless, this p.d.f. along with others, indicate the p.d.f. model of [3] in which the reaction zone is modelled as a flame sheet may provide a first approximation.

The evolution of the mean velocity, $\overline{U}$, for various flow conditions but constant flame angle, $\alpha = 24°$, is shown in Figure 6. For a given x, the location of the flame may be inferred from the increase in velocity due to heat release. The rate of acceleration decreases beyond the reaction zone as determined from the Rayleigh scattering.

For example, in Figure 6a, at x = 8.5 cm the velocity was found to begin to increase at y/d = 17.5 and the reaction zone thickness was 5.0 mm. The continued acceleration of the flow behind the flame results from the conversion of cross-stream to streamwise momentum. This occurs since the x-axis is aline of symmetry across which there can be no net mass flux. A similar interpretation holds for the other profiles.

In Figure 6a, at y/d = 1, x = 7.0 cm, there is a slight decrease in velocity due to the wake of the flame holder. Similar qualitative trends are exhibited in Figures 6b and 6c however, the effect of the wake is more pronounced due to the increased drag of the cylinder. The data of Figure 6c show clearly the existence of two competing processes which influence the flow pattern: 1) acceleration due to heat release and flow convergence, and 2) deceleration due to the drag of the flame holder. At relatively large flame angle α, corresponding to Figure 6, the effect of heat release and flow convergence is dominant. However, at smaller values of α, it would be expected that there would be less acceleration of the flow in the x-direction.

In Figure 7, mean profiles of the streamwise velocity component are presented for the condition corresponding to a flame angle of 12°, i.e. U = 684 cm/s and ϕ = 0.6. As expected the effect of the wake of the flame holder is dominant for this condition. No acceleration of the flow due to heat release is visible except at the farthest downstream locations. Rayleigh scattering indicated that for x = 8.0 cm, the mean flame position, as determined by the peak in the fluctuating intensity, is at y/d = 5.0. Bray and Libby [2], as discussed above, have assumed in modelling highly oblique flames that the streamlines

remain undeflected through the flame front. This imposes the kinematic condition that the velocity normal to the flame, U_n, is related to the velocity parallel to the flame front by the relation $U_p = U_n/\tan \alpha$, where α is the previously defined flame angle. The large component of velocity parallel to the flame produces a significant Reynolds stress in the flame which causes an increase in turbulent kinetic energy due to the interaction of this stress with the velocity gradient. The results presented in Figure 7 indicate these conditions to be invalid for our study since no increase in the streamwise component occurs, although for this flame angle this component is nearly parallel to the flame. We shall return to this point later in our discussion of turbulent kinetic energy.

The qualitative features of the flow fields described above are further emphasized by the profiles of turbulence intensity. In Figure 8, (U_∞ = 684 cm/s, ϕ = .75) at x = 8.5 cm, we see that for y/d > 16, the turbulence level is approximately 4.5%. Note that the turbulence intensity upstream of the flame increases slightly with increasing x. This systematically occurred for the other two conditions having the same flame angle, U_∞ = 500 cm/s, and 245 cm/s. As discussed previously in grid-generated turbulence, the turbulence intensity decays with increasing x. We presume that the slight increase shown here is due to fluctuations of the flame position and associated fluctuations in the upstream streamlines. At the flame, y/d = 14, there is a large increase in fluctuation intensity due to the movement of the flame front across the probe volume. The location of the peak and others in velocity fluctuation intensity are found to correlate well with the

locations of peak density fluctuations. Behind the flame the turbulence intensity decreases to approximately half of the level upstream of the flame. Thus a substantial decrease in turbulent kinetic energy occurs. This is consistent with the models [2,3] which suggest that dilatation effects will be dominant in flows propagating at relatively large angles to the upstream flow direction.

As in the case of Rayleigh scattering, the movement of the flame may be seen in terms of the velocity p.d.f. The p.d.f. of velocity is shown in Figure 9. As with the density p.d.f. a bimodal distribution occurs.

In Figure 10, profiles of turbulent velocity intensities are presented for $\alpha = 11°$. These profiles differ dramatically from those of Figure 8. The Rayleigh scattering indicated that the mean flame positions for x = 8.0 and 11.0 cm are respectively y/d = 5 and 11. No large increase in velocity fluctuation intensity at the flame is observed since no significant gradients of velocity are induced by the flame in the x-direction (Figure 7). The increase in turbulence intensity, at y/d = 3 is similar to that which is found in the wake of a cylinder in isothermal flow. The flame holder Reynolds number for this case is approximately 30, based upon the viscosity of the hot products, diameter of the flame holder and freestream velocity.

In order to determine the source of the maximum in turbulent velocity intensity, the power spectrum was calculated from the velocity time series at x = 11, y/d = 5. A peak at approximately 500 Hz was observed. The Strouhal number corresponding to this frequency is 0.07. Roshko [18] in a study of vortex shedding found that the Strouhal

number to be 0.12 for a circular cylinder of Reynolds number 40 in a flow without free stream turbulence. In this Reynolds number range, the Strouhal number decreases with decreasing Reynolds number; however, no vortex shedding is reported below this Reynolds number. Roshko [19] also reported vortex shedding from other bluff bodies and obtained a universal correlation based upon wake parameters such as the distance between free streamlines, and the velocity on the free streamline at separation. Since the wake at the flame holder is substantially altered by combustion, we can not compare our results with those reported for isothermal flows. It seems reasonable, however, to attribute the peak intensities shown in Figure 10 to vortex shedding from the flame holder since the frequency range is reasonable and the location of the intensity peaks are uncorrelated with flame position. It is possible that the correlation of Roshko [19] would predict the proper frequency if the effective "bluffness" of the cylinder-flame system could be determined (or alternatively, one might use the Roshko correlation to infer an effective "bluffness" for the cylinder-flame system).

The decrease of turbulent velocity intensity at y/d = 10, x = 11.0, seen in Figure 10, further confirms our observation that dilatation effects are dominant in determining the turbulent kinetic energy. The decrease in turbulent kinetic energy across the flame front is consistent with a flow with deflected streamlines and suggests that the predicted increase in kinetic energy through flames [2,3] is imply an artifact of the assumption of undeflected streamlines.

The qualitative features indicated for U_∞ = 684 cm/sec, ϕ = 0.6 and ϕ = 0.75 are both represented in results for the intermediate

condition U_∞ = 684 cm/s, ϕ = 0.7. The flame angle, as shown in Figure 3, is 18°. In Figure 11, mean velocity and turbulence intensity profiles are shown at x = 8.5 cm. Rayleigh scattering indicates the peak in density rms fluctuation occurs at y/d = 9. At y/d = 8, a peak in turbulence velocity intensity occurs due to the flame and the flow is accelerated due to the heat release of the flame. The peak in velocity intensity at y/d = 2 is associated with the wake of the flame holder. As in the previous cases, a decrease in turbulent kinetic energy occurs directly behind the flame.

Summary

Our study of flame propagation in grid-induced turbulence has indicated that for flames at relatively large angles to the upstream flow, the effect of heat release and flow dilatation is to decrease the turbulent kinetic energy. At smaller angles, the streamlines are deflected in such a manner that dilatation effects are still dominant. These data indicate that the deflection of streamlines at the flame must be accounted for in order to properly model the turbulent kinetic energy of flames. The effect of flame holder drag has also been shown to have a major effect on the flow field behind the flame, particularly with small flame angles. This suggests that results for such conditions are not typical of the interaction of a flame front with grid-induced turbulence. Probability density functions within the flame indicate that many features of density statistics may be interpreted in terms of flame sheet models. However, some errors will be introduced as a result of neglecting intermediate states.

Acknowledgements

This work was supported by AFOSR Contract F44620-76-C-0083. Additional equipment and facility support was provided by the Department of Energy, Basic Energy Science Division, Contract W-7405-ENG-48.

We wish to express our thanks to Mr. Bruce Ingraham for his assistance in programming for the computer controlled data acquisition system and for other data reduction assistance.

TABLE 1

U	Re_M	Equivalence Ratio ϕ	Flame Half Angle α
684	2280	.75	24
684	2280	.70	18
684	2280	.6	11
501	1670	.7	24
245	817	.55	24

REFERENCES

1. Damkohler, G. Z., Elektrochon, 46, 601 (1940); English translation, NACA Tech. Memo, 1112 (1947).

2. Bray, K.N.C. and Libby, P., Phys. Fluids, 19, 1687 (1976).

3. Libby, P. A. and Bray, K.N.C., AIAAJ, 15, 1186 (1977).

4. Clavin, P. and Williams, F. A., J. Fluid Mech., 90, 3 (1979).

5. Shchelkin, K. I., Soviet Phys.-Tech. Phys., 13 (1943).

6. Karlovitz, B., Denniston, D. W. and Wells, F. E., J. Chem. Phys. 19 (1951).

7. Richmond, J. K., Grumer, J. and Burgess, D. S., 7th Symposium (Int.) Combust., 615-620 (1960).

8. Smith, K. O. and Gouldin, F. C., Paper No. 77-183, presented at AIAA 15th Aerospace Sciences Meeting, Los Angeles, California (1977).

9. Andrews, G. E., Bradley, B. and Lwakabamba, S. B., Combustion and and Flame, 24, 285 (1975).

10. Namer, I., Schefer, R. W. and Chan, M., LBL-10655, Lawrence Berkeley Laboratory Report (1980).

11. Cheng, R. K., Bill, R. G., Jr., Robben, F., Schefer, R. and Talbot, L., Paper presented at 2nd Int. Symposium on shear layers, Imperial College, U.K. (1979).

12. Cheng, R. K., Bill, R. G., Jr. and Robben, F., to appear 18th Symposium (Int.) on Combustion.

13. Durst, F., Melling, A. and Whitelaw, J. H., Principles and Practice of Laser Doppler Anemometry, Academic Press, New York, 405 (1976).

14. Robben, F., LBL-3294, Lawrence Berkeley Laboratory Report (1975).

15. Batchelor, G. K. and Townsend, A., Proc. Roy. Soc., A, 193, 539 (1948).

16. Kármán, T. V., Proc. 5th Int. Cong. App. Mech. pp. 347-351 (1938).

17. Bennett, J. C. and Corrsin, S., Phys. Fluids, 21, 2129 (1978).

18. Roshko, A., NACA TN 2913 (1953).

19. Roshko, A., NACA TN 3169 (1954).

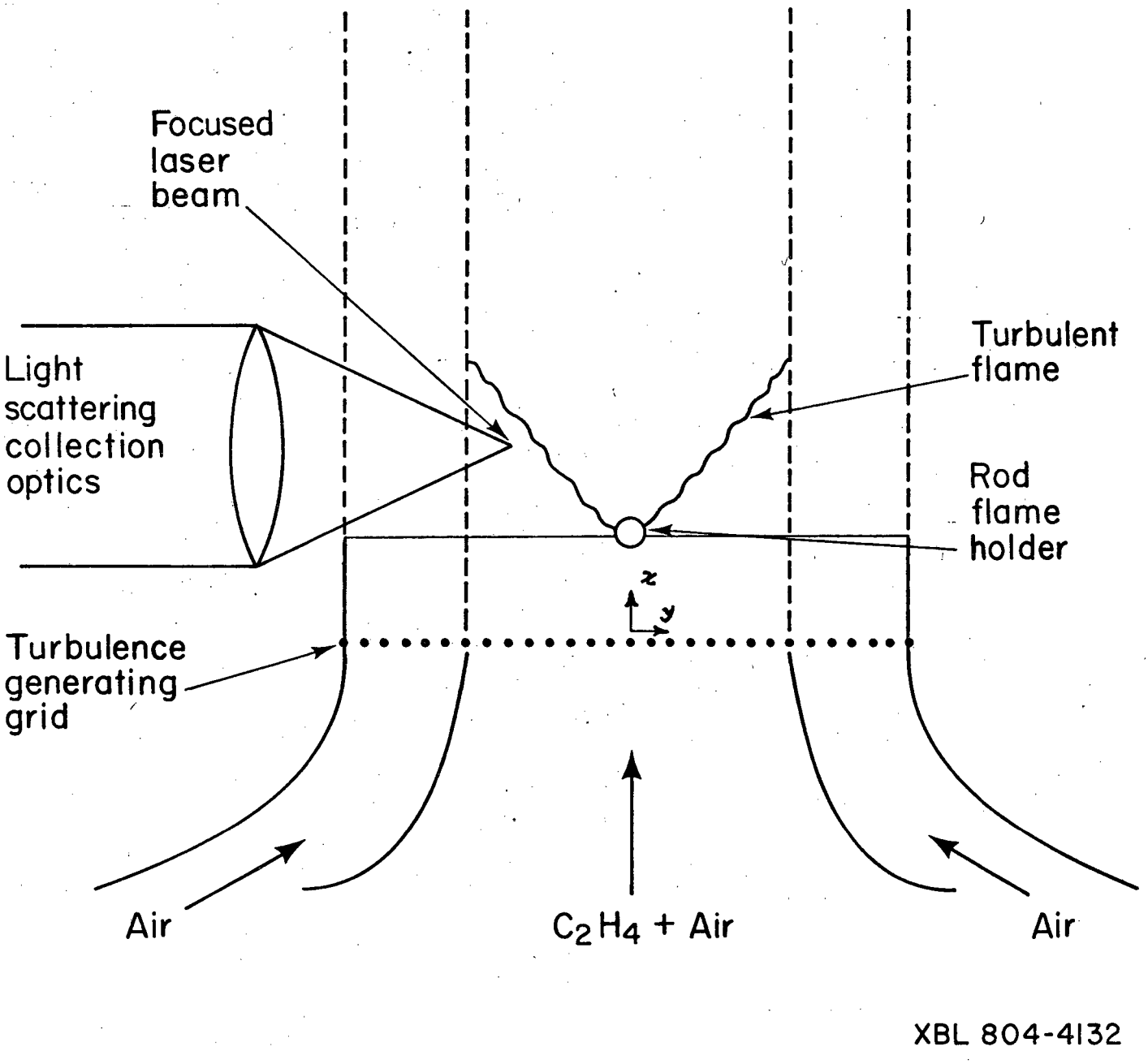

Figure 1 - Schematic of Flow System

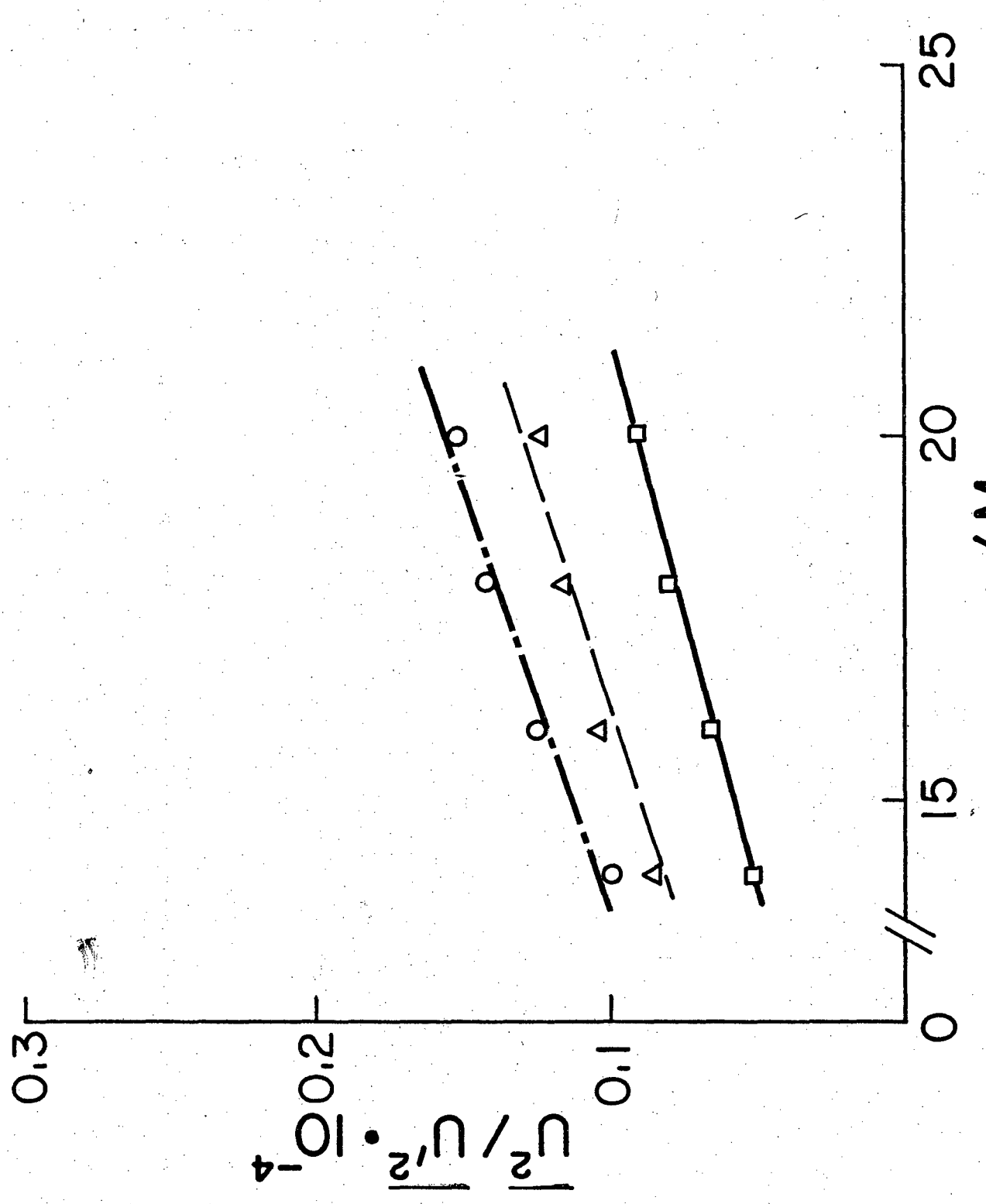

XBL 802-369

Figure 2 - Evolution of Grid-Generated Turbulence;
□ $\overline{U}$ = 245 cm/s; ○ - $\overline{U}$ = 501 cm/s; $\overline{U}$ = 684 cm/s

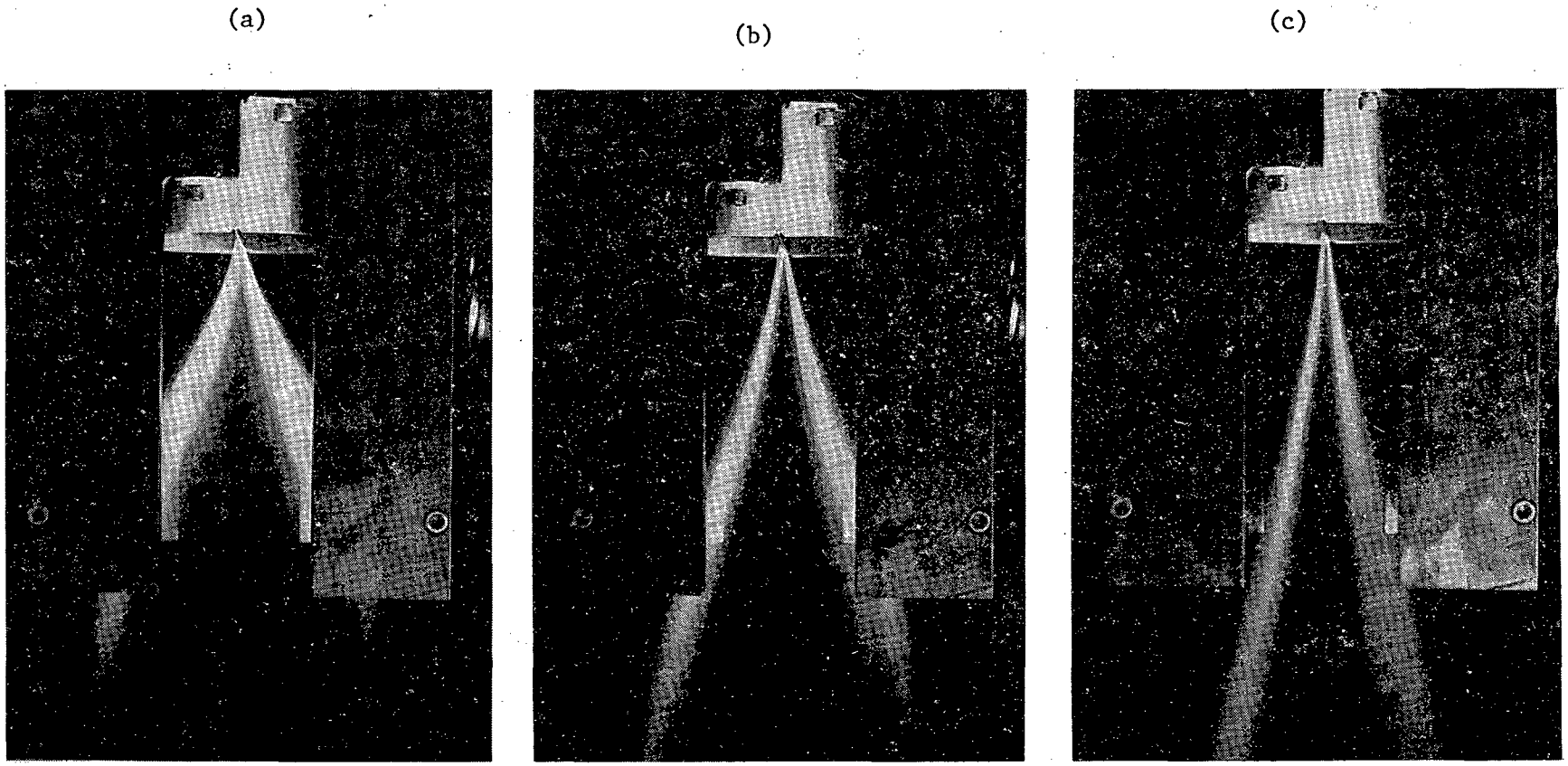

CBB 804-4642

Figure 3 - Flame propogation in grid induced turbulence: U=684 cm/s.
(a) ϕ = 0.6, (b) ϕ = 0.7, (c) ϕ = 0.75 .

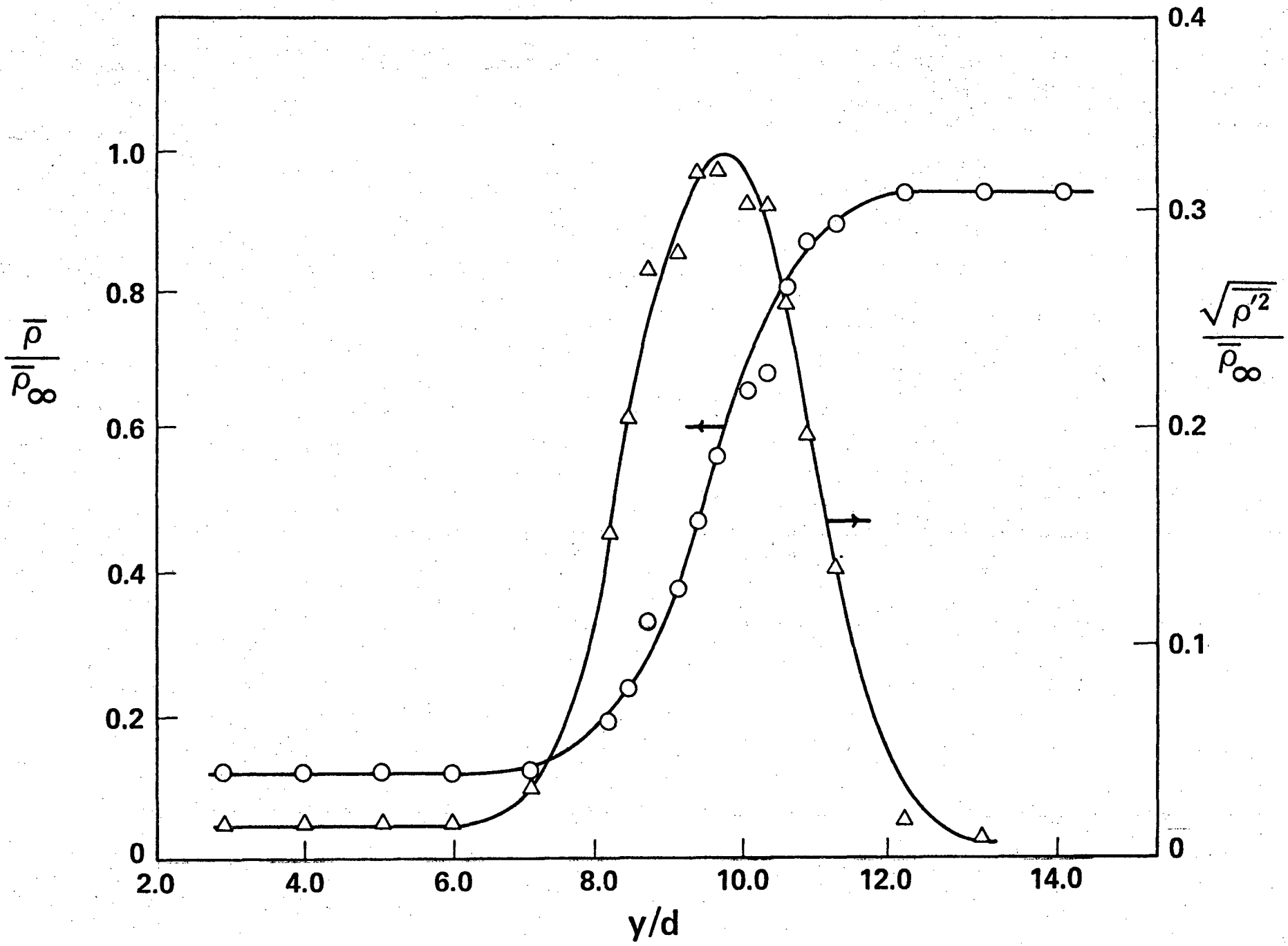

Figure 4 - Mean and RMS Intensity Profiles of Density; $\overline{u}_\infty$ = 684 cm/s, ϕ = .75, α = 24°, x = 7.5 cm.

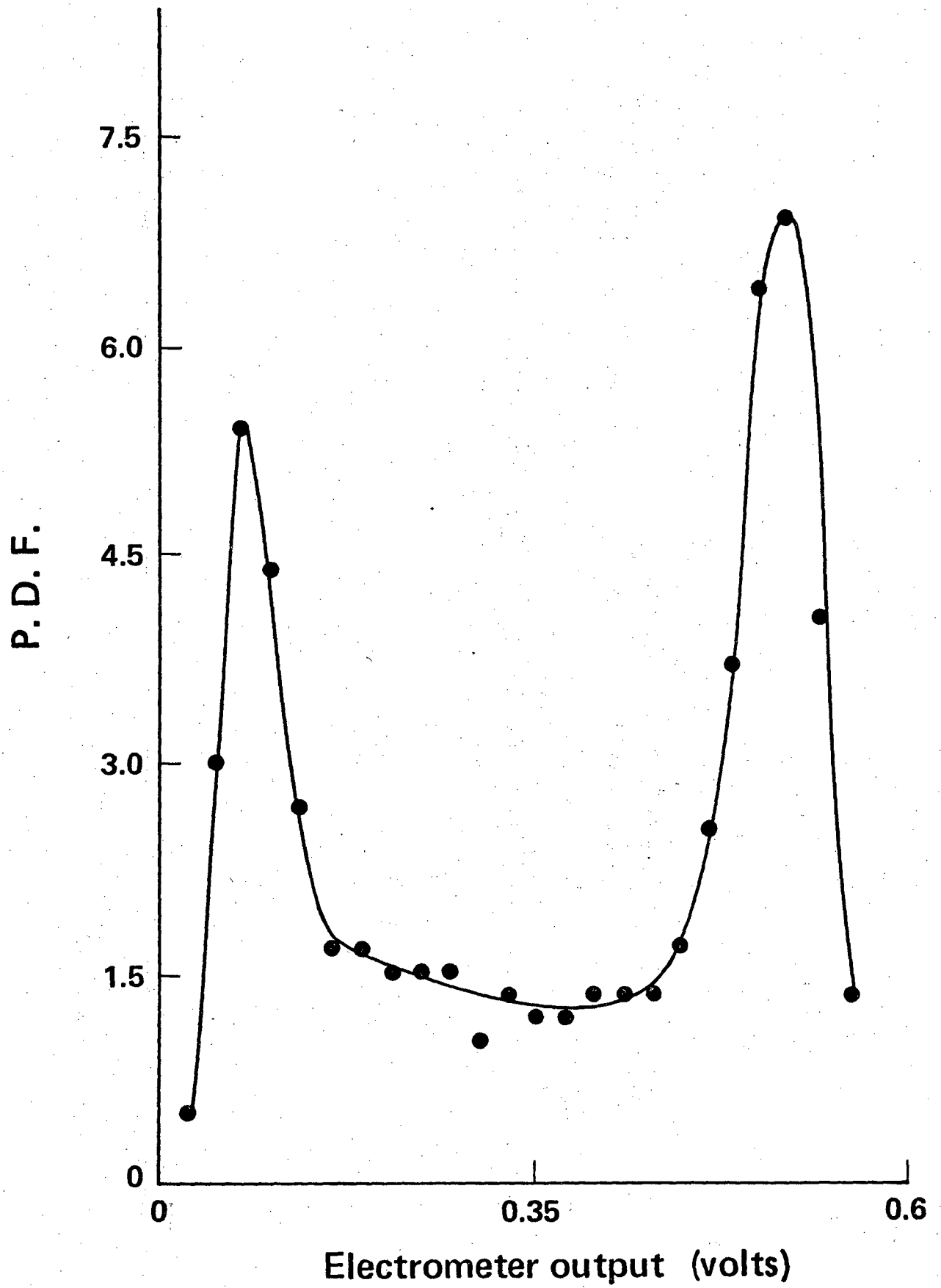

Figure 5 - Probability Density Function of Electrometer Output; $\bar{u}_\infty$ = 684 cm/s, ϕ = .75, α = 24°, x = 7.5 cm, y/d = 10.

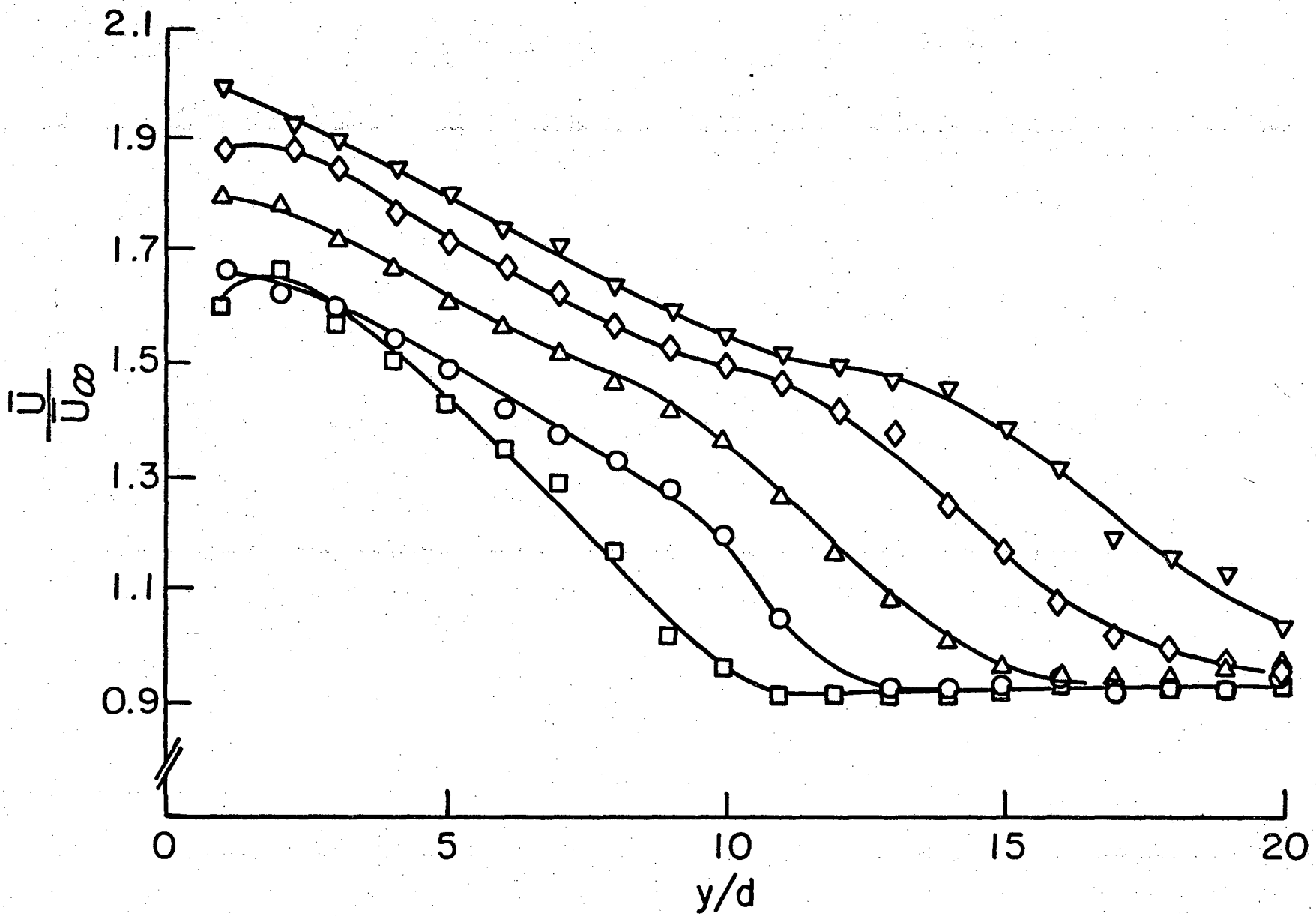

Figure 6a - Mean Velocity Profiles Through a Flame;
$\overline{U}_\infty$ = 245 cm/s, ϕ = .55, α = 24°
□ x = 7.0 cm, ○ x = 7.5 cm, △ x = 8.0 cm, ◇ x = 8.5 cm, ▽ x = 9.0 cm.

XBL 802-366

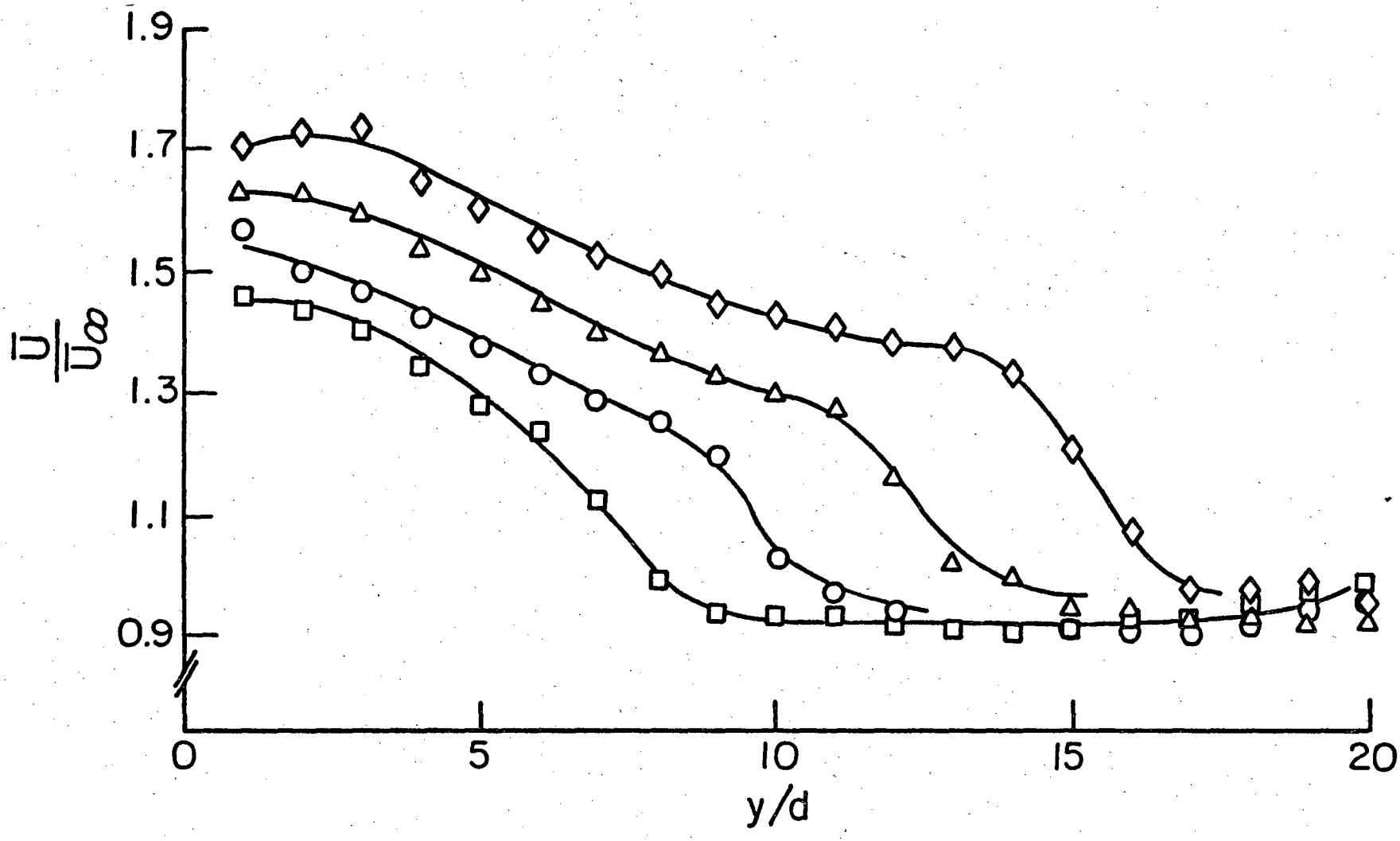

Figure 6b - Mean Velocity Profiles Through a Flame;
U_∞ = 501 cm/s, ϕ = .70, α = 24°;
□ x = 7.0 cm, ○ x = 7.5 cm, Δ x = 8.0 cm, ◇ x = 8.5 cm.

XBL802-387

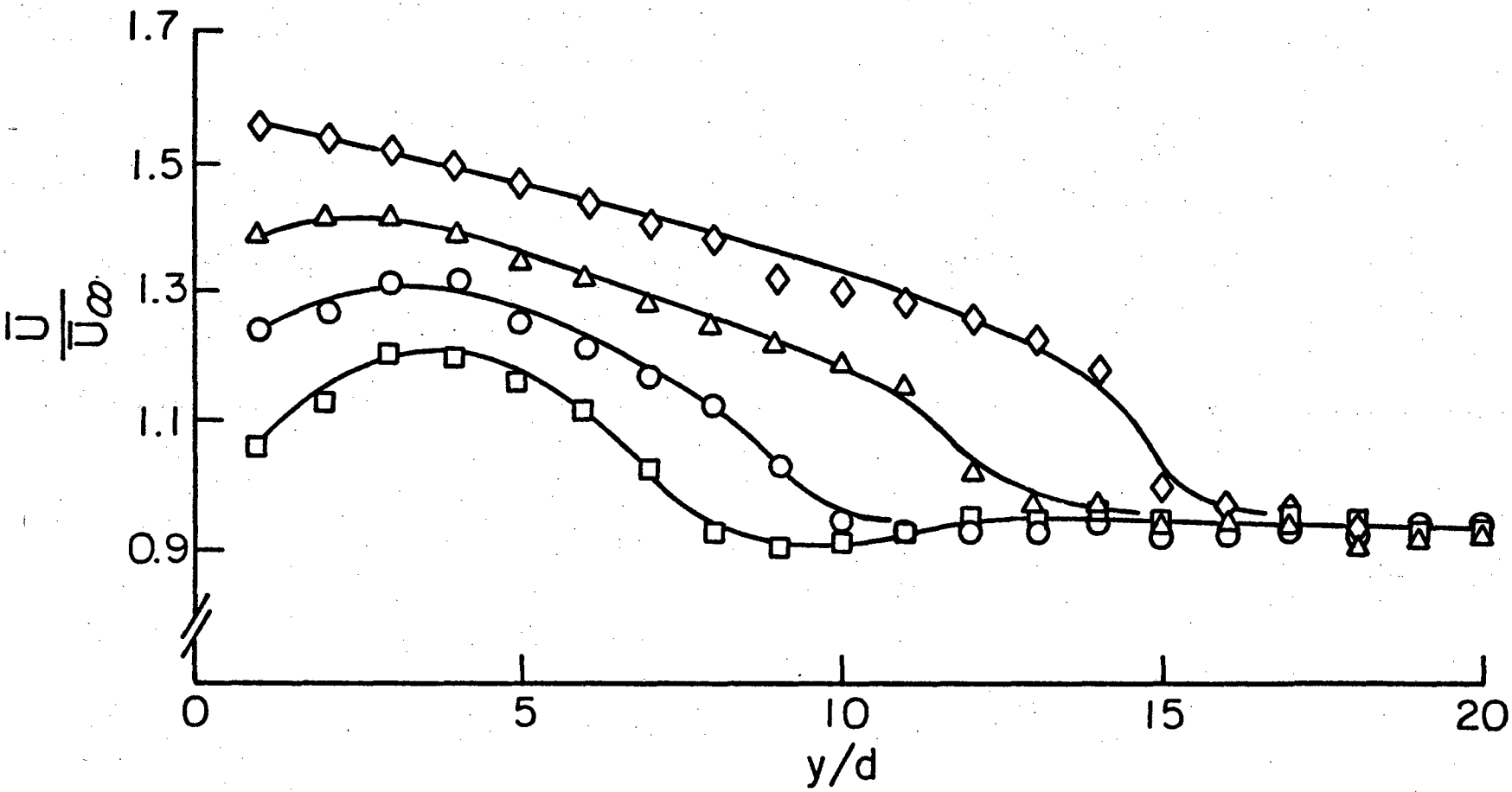

Figure 6c - Mean Velocity Profiles Through a Flame;
U_∞ = 684 cm/s; ϕ = .75, α = 24°; □ x = 7.0 cm, ○ x = 7.5 cm,
Δ x = 8.0 cm, ◇ x = 8.5 cm.

XBL 802-368

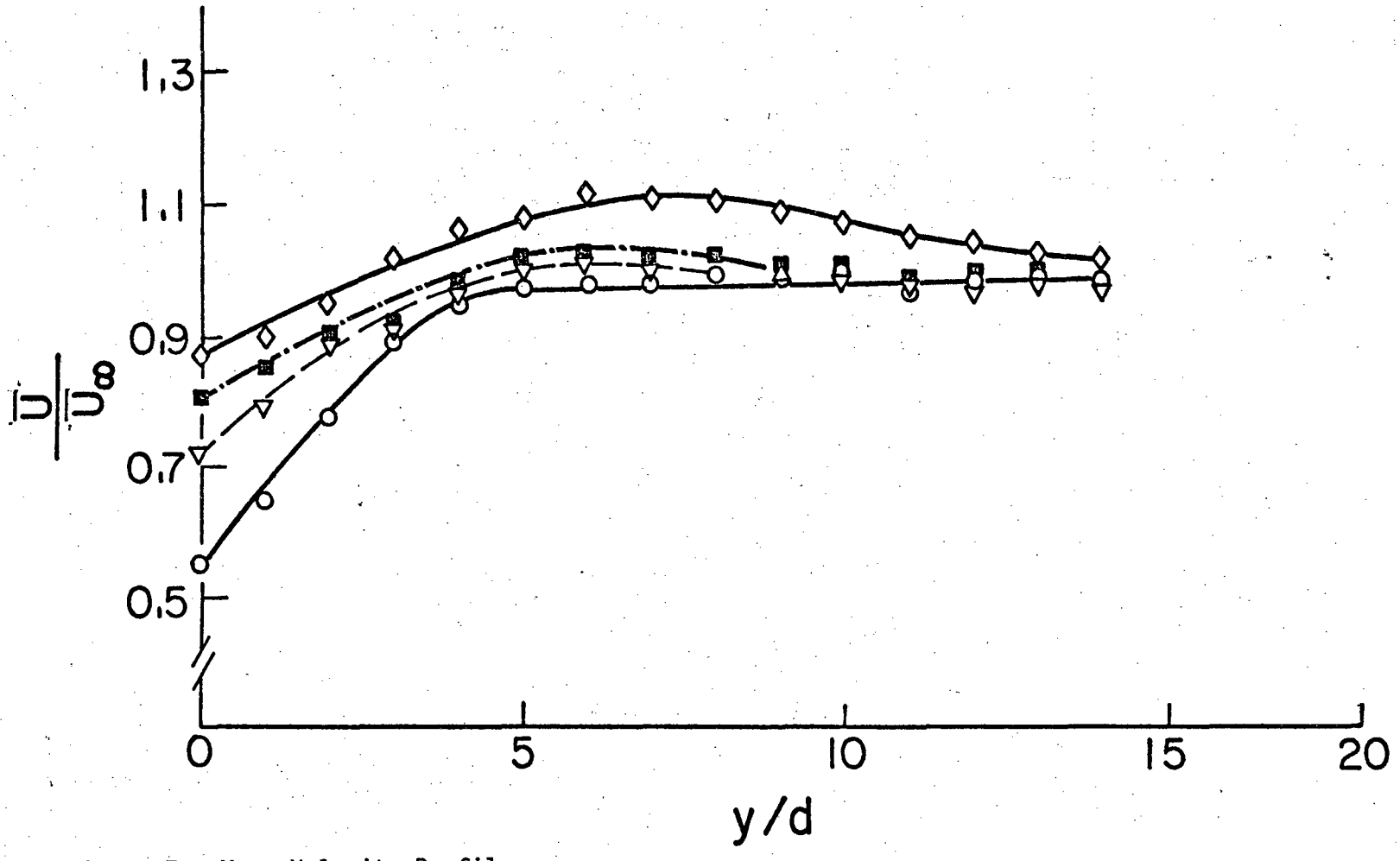

Figure 7 - Mean Velocity Profiles;
$\overline{U}_\infty$ = 684 cm/s, ϕ = .60, ϕ = 12°,
○ x = 8.0 cm, ▽ x = 9.0 cm, ■ x = 10.0 cm, ◇ x = 11.0 cm.

XBL802-367

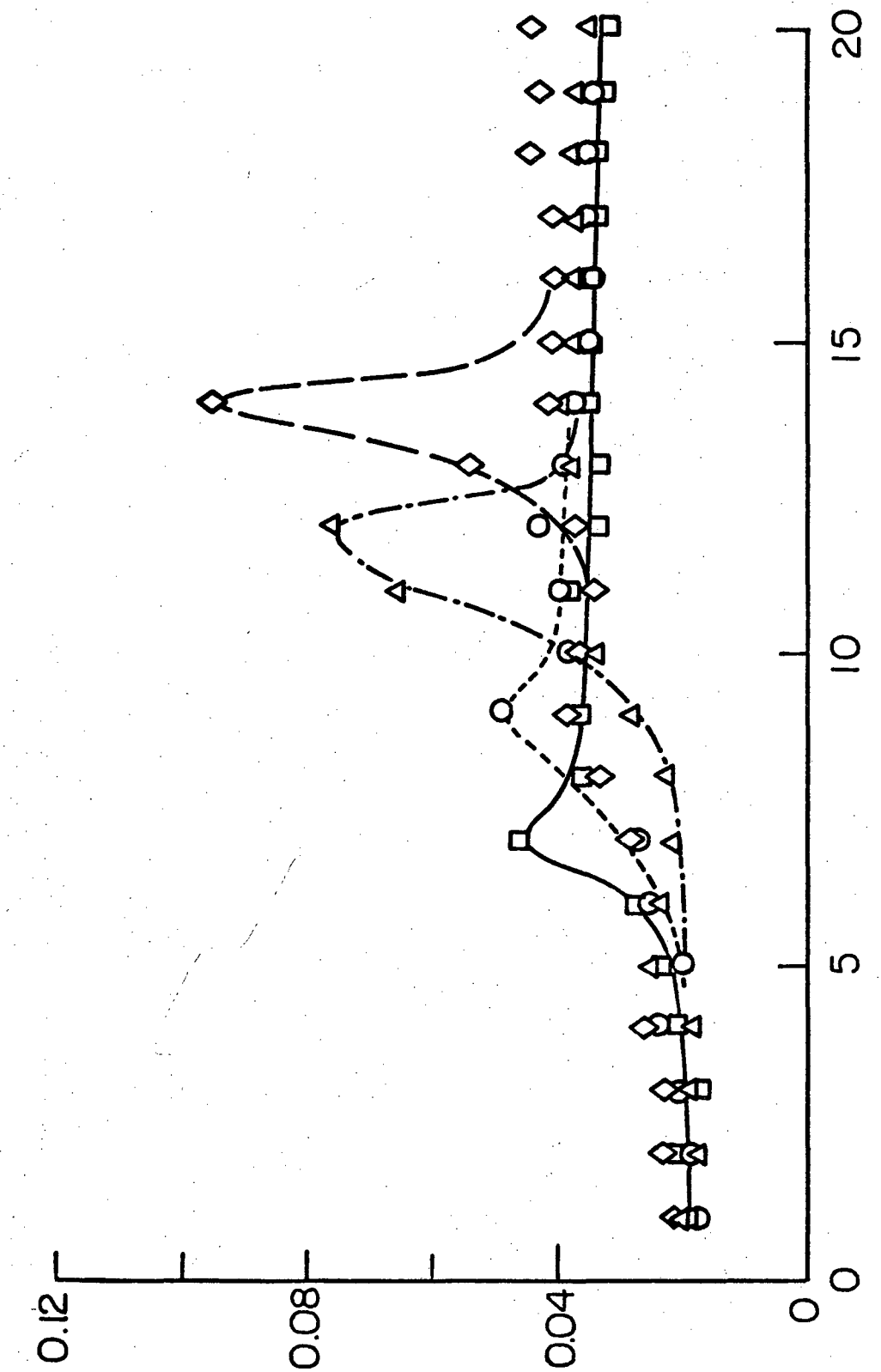

Figure 8 - Turbulence Intensity Profiles;
U_∞ = 684 cm/s, ϕ = .75, α = 24°,
□ x= 7, ○ x = 7.5, Δ x = 8.0, ◇ x = 8.5 cm.

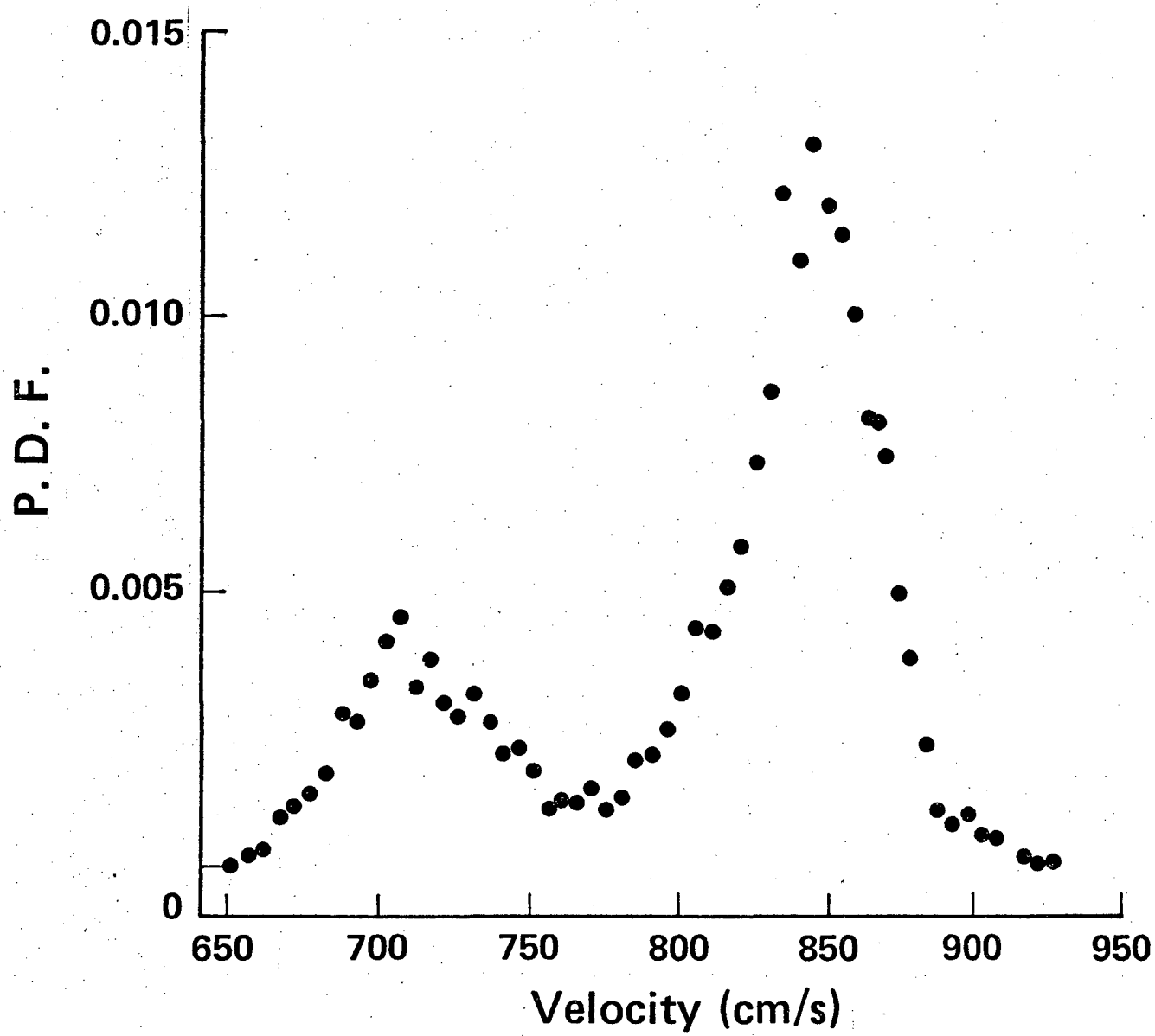

Figure 9 - Probability Density Function of Velocity;
U_∞ = 684 cm/s, ϕ = .75, α = 24°, x = 8.5 cm, y/d = 13.

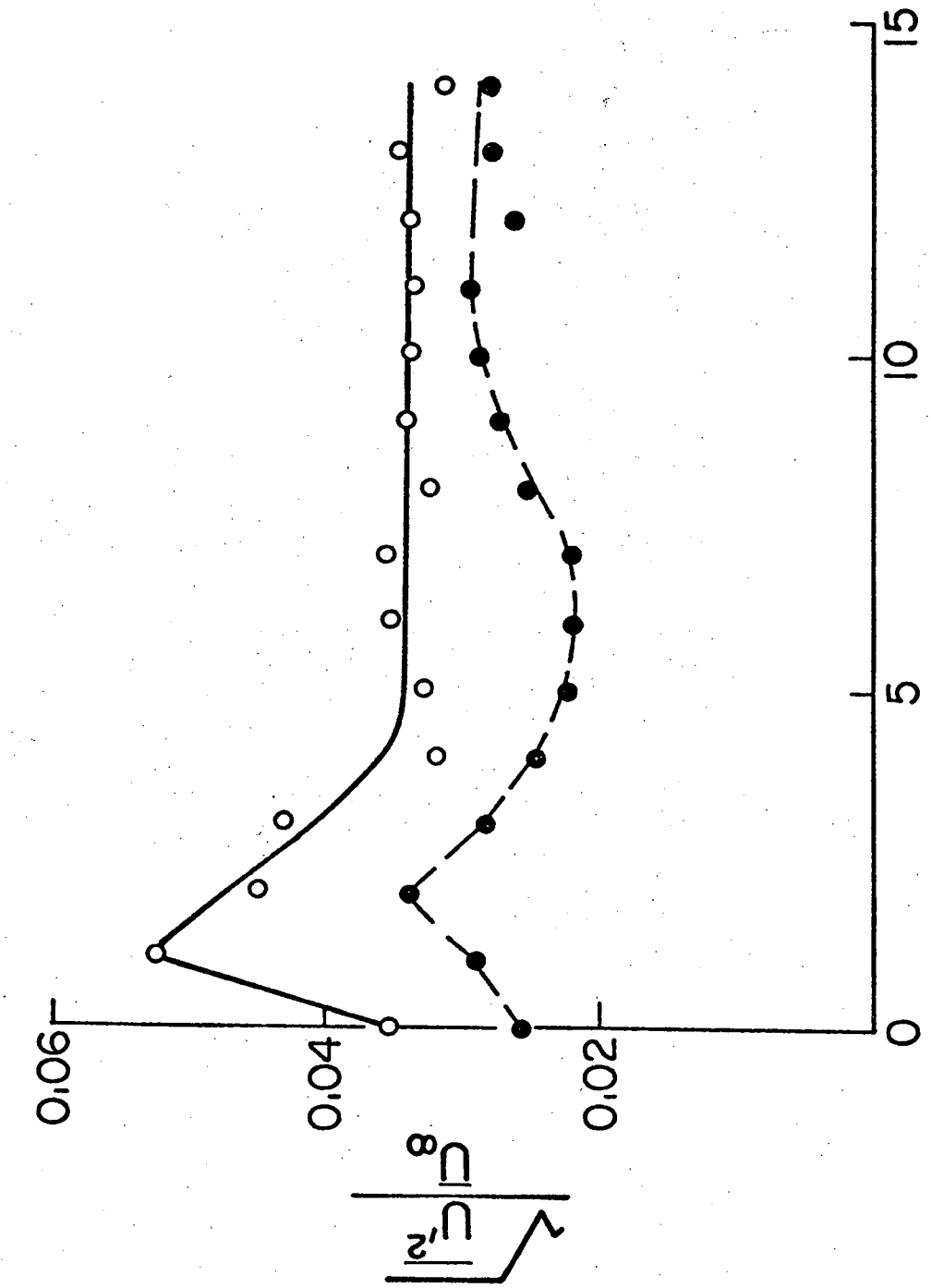

XBL802-372

Figure 10 - Turbulence Velocity Intensity;
U_∞ = 684 cm/s, ϕ = 0.6, α = 12°, ○ x = 8.0, ● x = 11.0 cm.

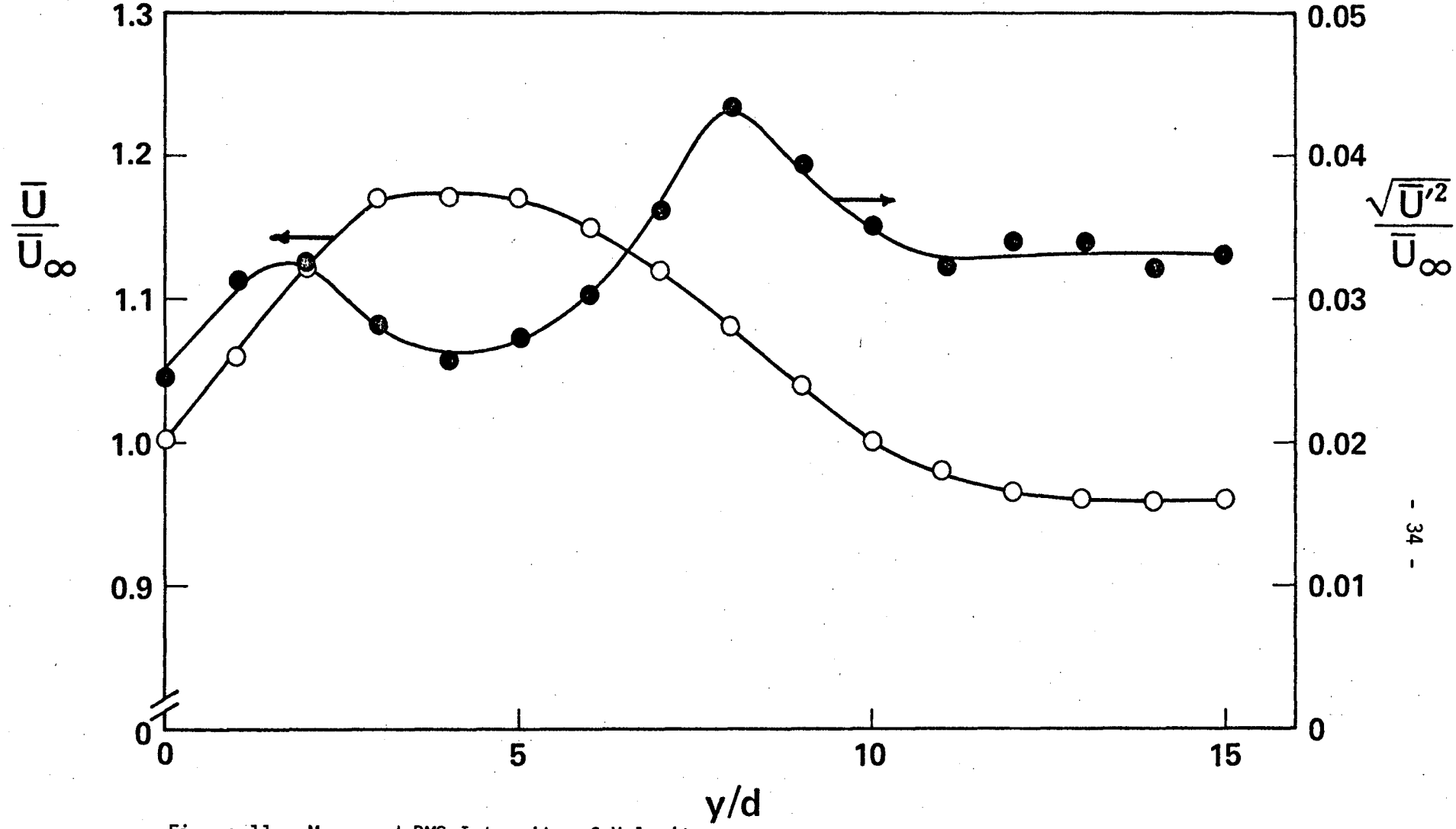

Figure 11 - Mean and RMS Intensity of Velocity;
U_∞ = 501 cm/s, ϕ = .70, α = 18°, x = 8.5 cm.

TECHNICAL INFORMATION DEPARTMENT
LAWRENCE BERKELEY LABORATORY
UNIVERSITY OF CALIFORNIA
BERKELEY, CALIFORNIA 94720